Morphology control and optical properties of ZnO nanostructures grown by ultrasonic synthesis

N. Morales-Flores[1a], R. Galeazzi[1b], E. Rosendo[1c], T. Díaz[1d], S. Velumani[2e] and U. Pal[*3]

[1]*Centro de Investigación en Dispositivos Semiconductores, ICUAP, Benemérita Universidad Autónoma de Puebla, Puebla, Pue. 72570, Mexico*
[2]*Department of Electrical Engineering (SEES), Centro de Investigación y de Estudios Avanzados del IPN, Av. Instituto Politécnico Nacional # 2508, Col. San Pedro Zacatenco, 07360 Mexico D.F., Mexico*
[3]*Instituto de Física, Benemérita Universidad Autónoma de Puebla, Apdo. Postal J-48, Puebla, Pue. 72570, Mexico*

(Received January 15, 2013, Revised April 3, 2013, Accepted April 4, 2013)

Abstract. ZnO nanostructures of rod-like, faceted bar, cup-end bars, and spindle shaped morphologies could be grown by a low power ultrasonic synthesis process. pH of the reaction mixture seems to plays an important role for defining the final morphology of ZnO nanostructures. While the solution pH as low as 7 produces long, uniform rod-like nanostructures of mixed phase (ZnO and $Zn(OH)_2$), higher pH of the reaction mixture produces ZnO nanostructures of different morphologies in pure hexagonal wurtzite phase. pH of the reaction as high as 10 produces bar shaped uniform nanostructures with lower specific surface area and lower surface and lattice defects, reducing the defect emissions of ZnO in the visible region of their photoluminescence spectra.

Keywords: ZnO; nanostructure; ultrasound synthesis; morphology control; optical properties

1. Introduction

Size and shape controlled synthesis of semiconductor nanostructures has attracted considerable attention recent yeras as their physical and chemical properties depend strongly on morphology, size, and dimensions (Alivisatos *et al*. 1996, Xia *et al.* 2003, Zhang *et al.* 2002). ZnO is one of the most promising multifunctional semiconductors with wide direct band gap energy (3.37 eV at 300 K) and large exciton binding energy (60 meV). In nanostructure form, ZnO reveals a wide range of growth morphologies, such as nanoring, nanowire, nanotube, nanohelix, nanobelt, nanocage,

∗Corresponding author, Professor, E-mail: upal@sirio.ifuap.buap.mx
[a]Research Scholar, E-mail: natalia12-1@hotmail.com
[b]Professor, E-mail: ingquim25@gmail.com
[c]Professor, E-mail: enrique171204@gmail.com
[d]Professor, E-mail: tomas.diaz.be@gmail.com
[e]Professor, E-mail: vels64@yahoo.com

nanosphere, nanorod, and nanodisk (Pal *et al.* 2005, Xu *et al.* 2004, Escobedo-Morales *et al.* 2008). ZnO nanostructures have received broad attention due to their distinguished performance in the fields of electronics, optics, photonics and catalysis, particularly for applications such as light emitting diode, laser, field emission device, chemical sensor, and catalyst (Lee *et al.* 2005, Huang *et al.* 2001, Zhu *et al.* 2003, Fan *et al.* 2005, Morales-Flores *et al*. 2011). Several methods have been applied to synthesize ZnO nanostructures of different morphologies including wet chemical methods, thermal evaporation, physical vapor deposition, metal–organic chemical vapor deposition (MOCVD), molecular beam epitaxy (MBE), pulsed laser deposition and sputtering (Laudise *et al.* 1960, Pal *et al.* 2001, Yao *et al.* 2002, Chiou *et al.* 2003, Venkatachalam *et al.* 2010).

Recently, sonochemical method has been proposed as a promising alternative technique for the fabrication of ZnO nanostructures under ambient conditions (Zhang *et al.* 2005, Pu *et al.* 2007, Bhattacharyya *et al.* 2008, Pal *et al.* 2009). The method is fast, simple, economical, and environmentally benign (Suslick *et al.* 1996, Mishra *et al.* 2009, Dhas *et al.* 2005). In sonochemical synthesis, the chemical effects of ultrasound arise from acoustic cavitation phenomena, i.e., the formation, growth and implosive collapse of the bubbles in liquid media (Kumar *et al.* 2000). The implosive collapse of the bubbles generates localized hot spots (temperature $\approx$ 5000 K, pressure $\geq$1000 atm, and cooling rate $>10^9$ K/s).

In this article, we report on the synthesis of ZnO nanostructures of different morphologies using a low power sonochemical technique utilizing water as solvent. Effects of pH variation on the morphology, structure and photoluminescence (PL) characteristics of the nanostructures have been discussed.

2. Experimental

ZnO nanostructures were synthesized through a facile sonochemical route. For this purpose, a 0.068 M zinc acetate solution was prepared by dissolving 3g of zinc acetate dihydrate [$Zn(CH3COO)_2 \bullet 2H_2O$, Baker, 99.9%] in 200mL of deionized (DI) water at room temperature under vigorous stirring. Then an appropriate amount of ammonium hydroxide (NH_4OH) was slowly added into it until the pH of the mixture solution reaches a desired value. The solution was kept under stirring for another 15min. The resulting solution was kept under ultrasonic irradiation using a T-horn ultrasonic processor (UP400S, Hielscher, 400 Watt, 24 kHz) at 40W dissipated power under argon gas flow for 3 h. Finally, the obtained product was centrifuged and washed several times with ethanol at 8000rpm for 10 minutes and dried at 70°C for 6 hours in a muffle furnace, obtaining powder samples. Several samples were prepared under similar conditions varying only the pH value of the reaction mixture in between 7 and 10.

All the samples were analyzed by scanning electron microscopy (JEOL JSM 5600LV), X-ray diffraction (XRD) (Bruker AXS D8 Discover diffractometer, with monochromatic CuKα radiation, =1.5406 Å, operating at 40 kV, 40 mA), diffuse reflectance spectroscopy (DRS) in UV-Vis spectral range, and room temperature Raman spectroscopy (LabRAM HR-Olympus Micro Raman system) in backscattering configuration using the 633 nm line of a He-Ne laser as excitation source. The room temperature photoluminescence (PL) spectra of the samples were recorded using a 1m long ScienceTech monochromator and 325 nm emission of a He-Cd laser as excitation source (5mW). A Hamamtsu (model PMH-04) photomultiplier tube was utilized as detector. For determining the specific surface area of the samples, their nitrogen adsorption-

desorption isotherms at 77K were recorded in a Belsorp-Mini II (BEL Japan, Inc) analyzer. Before recording their isotherms, the samples were degassed at 250°C for 5h in vacuum prior to the measurements.

3. Results and discussion

Fig. 1 shows typical SEM images of the ZnO nanostructures grown at different pH values (7-10) of the reaction mixture. A strong influence of solution pH on the growth morphology of the nanostructures can be clearly observed from the micrographs. While ZnO nanorods of about 86 nm average width and 1200 nm average length were formed (Fig. 1(a)) for pH 7 of the reaction mixture, formation of faceted nanobars and nanocups of 250-430 nm average lengths and 180-280 nm average widths could be observed for the higher pH values (Figs. 1(b)-1(d)). As can be seen, the morphology and the average size of the nanostructures change drastically with the increase of solution pH.

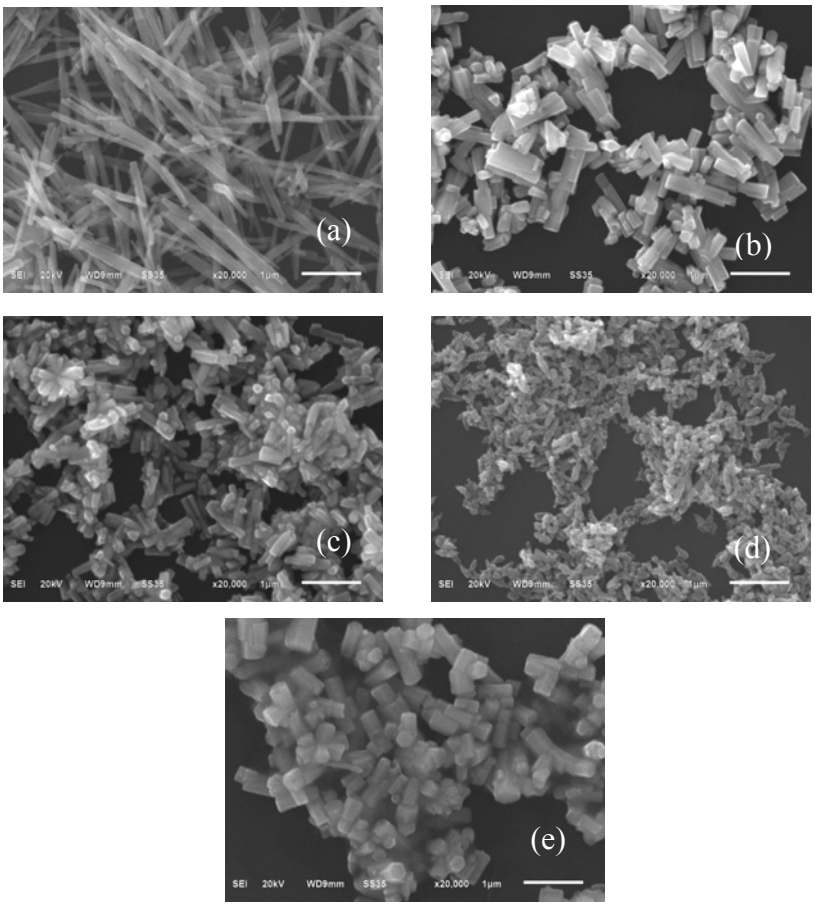

Fig. 1 Typical SEM micrographs of the ZnO nanostructures grown at (a) pH 7, (b) pH 7.5, (c) pH 8, d) pH 9, and (e) pH 10 of the reaction mixture

Fig. 2 shows the XRD patterns of the ZnO nanostructures grown at different pH values of the reaction mixture. The diffraction patterns exhibit all the characteristic peaks of ZnO in hexagonal wurtzite phase (JCPDS card # 089-1397). However, for the sample prepared at pH 7, there appeared several diffraction peaks associated to $Zn(OH)_2$ phase, indicating the formation of $Zn(OH)_2$ in neutral reaction condition. At neutral pH condition of the reaction mixture, a large quantity of zinc hydroxide nuclei are produced, while the number of available growth units is small to obtain ZnO nanostructures (Xu *et al.* 2011, Demianets *et al.* 2002). No characteristic diffraction peaks associated to other structural phase or impurity could be detected in the samples grown in between pH 7.5 and pH 10 of the reaction mixture. The intensity of the diffraction peaks is found to increase with the increase of pH value, suggesting that higher pH value helps the nucleation and grain growth of ZnO nanostructures.

The crystallite size (t) in the ZnO nanostructures was calculated using Debye Scherer formula (Cullity 1956) on their (101) diffraction peaks

$$t = \frac{K\lambda}{B\cos\theta} \tag{1}$$

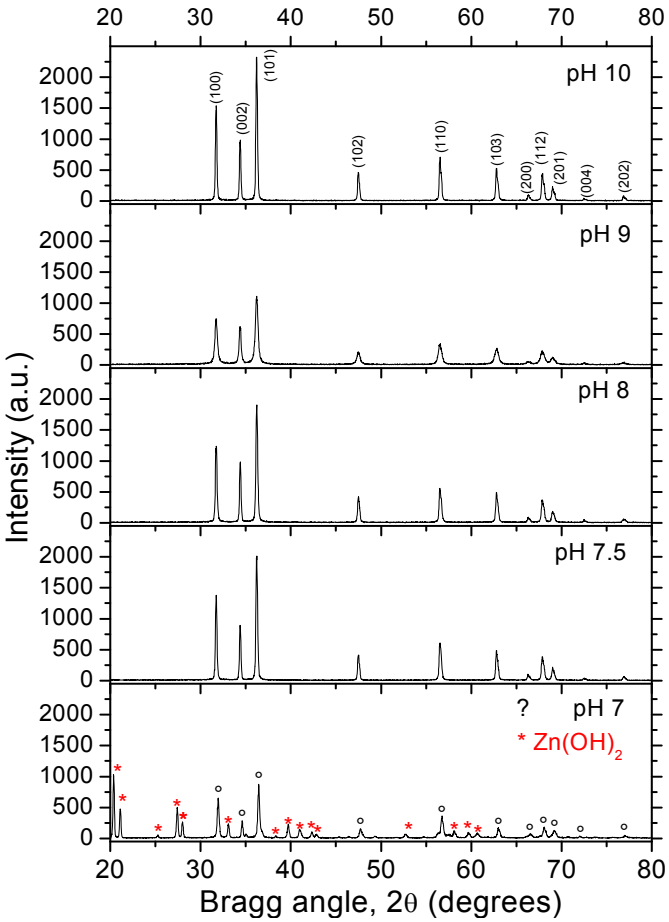

Fig. 2 XRD patterns of the ZnO nanostructures grown at different pH values

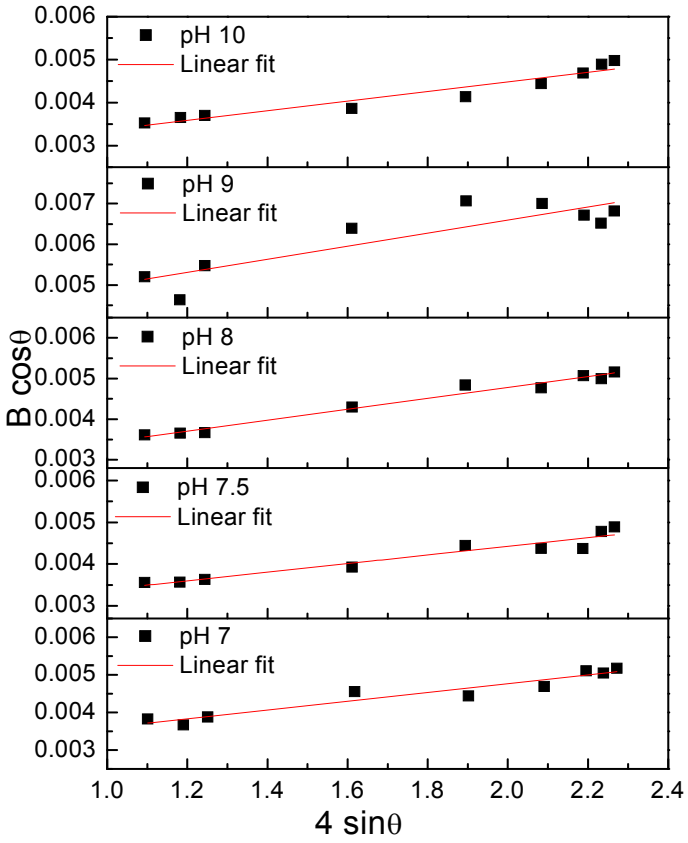

Fig. 3 Williamson-Hall plots for the ZnO nanostructures grown at different pH values of the reaction mixture

Table 1 SEM estimated dimensions, XRD estimated average particle size and microstrain, and BET specific surface area of the ZnO nanostructures grown at different pH values of the reaction mixture

pH of the reaction mixture	Observed morphology	Avg. length (nm)	Avg. width (nm)	Avg. crystallite size (nm)	BET specific surface area (m^2/g)	Microstrain
pH 7.0	rods-like	1182±285	86±19	38	----	----
pH 7.5	faceted bars	431±73	183±8	38	4.48	0.00108
pH 8.0	Cup-end bars	389±30	135±7	35	6.15	0.00134
pH 9.0	spindles	256±33	95±13	23	12.61	0.00161
pH 10.0	faceted bars	407±23	278±34	38	4.29	0.00112

where K is the shape factor (depends on the shape of the particles), considered to be 0.9, λ is the wavelength of used X-ray (λ=1.5406 Å), B is the full width at half maximum (FWHM) of the (101) peak, and θ is the Bragg angle. Estimated average crystallite size values for the ZnO nanostructures grown at pH 7, 7.5, 8, 9 and 10 were about 38, 38, 35, 23 and 38 nm, respectively (Table 1).

To monitor the effect of solution pH on the lattice deformation, microstrain and crystallite size of each sample, we utilized Williamson-Hall equation (Venkateswara *et al.* 2008)

$$B\cos\theta = \frac{K\lambda}{t} + 2\varepsilon\sin\theta, \tag{2}$$

where *B, θ,* λ, t and *K* are the same parameters utilized in equation 1, and ε is the microstrain in the nanocrystals. Using Williamson-Hall plots (B cosθ vs. 4 sinθ, Fig. 3) the microstrain vales for the samples prepared at different pH values were estimated and presented in Table 1. As can be observed, on increasing the pH of the reaction solution, average crystallite size of the samples decreases and microstrain in their crystal lattice increases gradually up to pH 9. However, a sudden increase of crystallite size and a decrease of microstrain were observed for the sample grown at pH 10. Obtained results clearly indicate that the pH variation affects the crystal lattice, increasing tensile strain in the ZnO nanostructures with the increase of basicity of reaction solution. Variation of ZnO nanostructure morphology with the variation of solution pH has already been demonstrated by several researchers (Pal and Santiago 2005, Wahab *et al.* 2009) and explained through the variations of H^+ and OH^- ion concentration in reaction solution and their effects on the growth rates of different polar and nonpolar planes. However, in the present case, not only the pH of the reaction mixture was varied, the hydrolysis process was performed under the influence of ultrasonic irradiation, and the obtained ZnO nanostructures had quite different morphologies than the morphologies reported by non-ultrasonic processes.

On the other hand, to estimate the texture properties, nitrogen adsorption-desorption isotherms of the samples were recorded (Fig. 4). N_2 adsorption-desorption behaviors of all the samples corresponded to type III isotherm in Brunauer classification. The characteristic feature of these curves is their hysteresis loop, which does not exhibit any limiting adsorption at high relative pressures (Jing *et al.* 2008). The Brunauer-Emmett-Teller (BET) specific surface area of the nanostructures were calculated to be 4.48, 6.15, 12.61 and 4.29 $m^2\ g^{-1}$ for the samples grown at pH values 7.5, 8, 9, and 10, respectively (Table 1). As can be seen, on increasing the pH of the reaction mixture (up to 9) while the crystallite size of the samples decreases, their BET specific surface area increases as one can expect. However, a sudden decrease of BET specific surface area is observed for the sample grown at pH 10.

Fig. 5 presents Raman spectra of the ZnO nanostructures grown at different pH values of the reaction mixture. For wurtzite ZnO, occurrence of six first-order vibrational modes, named A_1, E_1, $2E_2$, and $2B_1$ can be expected near the Γ point of its first Brillouin zone (Arguello *et al.* 1969). The A_1 and E_1 modes are polar in nature, and split into transverse- (TO) and longitudinal optical (LO) phonon modes. The E_2 modes (E_2^{low}, E_2^{high}) are non-polar and Raman active. The B_1 modes are infrared active, normally do not reveal in Raman spectra. The Raman spectrum of the ZnO sample prepared at pH 7 revealed peaks located at about 375 and 445 cm^{-1}, which are attributed to the A_1(TO) and E_{2H} modes of wurtzite ZnO, respectively (Fig. 5(a)). There appeared five more peaks, located at about 220, 266, 486, 554 and 725 cm^{-1} which correspond to $Zn(OH)_2$ phase (Vargas-Hernández *et al.* 2009, Zhou *et al.* 2002). Raman spectra of the samples prepared at higher pH values (7.5- 10) revealed seven peaks (Fig. 5(b)), located at about 100, 205, 333, 380, 439, 572 and 665 cm^{-1}. While the peak centered at about 100 cm^{-1} is attributed to E_{2L} mode of wurtzite ZnO, the peaks revealed around 439 and 572 cm^{-1} are attributed to the E_{2H} and A_1(LO) modes of wurtzite ZnO, respectively. The peaks centered at about 205 and 333 cm^{-1} have been previously observed in ZnO by several researchers (Phan *et al.* 2008, Kumar Yadav *et al.* 2007, Serrano *et al.* 2004),

and were attributed to higher order fundamental modes or multiphonon modes. The peak located at 665 cm^{-1} was attributed to (TA+LO) mode of ZnO (Wang *et al.* 2007, Jang *et al.* 2009). In the nanostructures, the E_{2H} Raman peak associated to oxygen sub-lattice of ZnO became broader and less intense with the increase of pH value, which might be due to the incorporation of disorder in ZnO lattice during the their growth at faster rate at higher pH values.

The UV-Vis diffuse reflectance spectra of the ZnO samples grown at different pH values are presented in Fig. 6. All the spectra revealed a sharp absorption edge at around 375 nm, characteristic of crystalline ZnO. While the position of absorption edge did not change noticeably, the reflectance of the samples in the visible spectral range (500-700 nm) decreased gradually with the increase of pH value of the reaction mixture. The band gap energy (E_g) of the samples was estimated from the intersection of the linear fits of the Kubelka–Munk (KM) transformation of their reflectance spectra (Fig. 6(b)) with the energy axis (Escobedo-Morales *et al.* 2007). As can be seen from figure 6b, the pH of the reaction mixture has no significant influence on the band gap energy of the ZnO nanostructures. The band gap energy estimated for the samples grown at solution pH 7, 7.5, 9, and 10 were 3.31, 3.28, 3.31 and 3.27 eV, respectively.

Fig. 7 shows the room temperature PL spectra of ZnO nanostructures grown at different pH

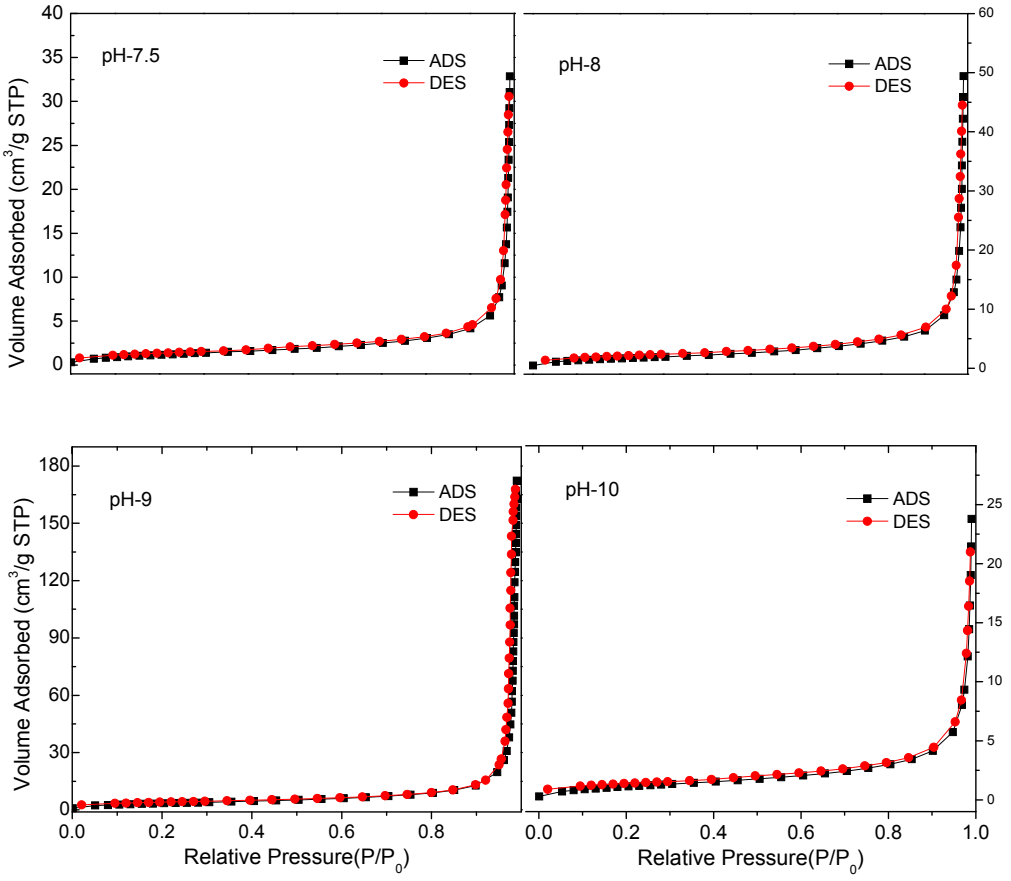

Fig. 4 N_2 adsorption/desorption isotherms of the ZnO nanostructures grown at different pH values

values, normalized to their excitonic (UV) emissions. PL spectra of all the samples revealed two emission bands. While the ultraviolet (UV) emission around 380 nm generally assigned as the near band edge emission attributed to excitonic transition, the broad and intense emission in the visible region (centered around 580 nm) is associated with structural defects and impurities of different natures. Commonly this broad visible emission contains several components assigned as red (1.75 eV), orange (1.95 eV), yellow (2.20 eV), green (2.40 eV), and blue (2.60 eV) emissions; each associated to particular defect or defect complex in the electronic band gap of ZnO. While the green emission has been associated to oxygen vacancies (V_O), the orange emission has been associated to oxygen in excess or interstitial oxygen (O_i), interstitial zinc (Zn_i), and impurities like Li ions (Hsu *et al.* 2006, Studenikin *et al.* 1998). Origins of red and blue emissions are not very clear and controversial. However, they are believed to be associated with the shallow V_O and Zn_i levels, respectively (Wei *et al.* 2007, Jannoti *et al.* 2007). On the other hand, the yellow emission has been suggested to be associated with interstitial oxygen O_i^- (Wu *et al.* 2001).

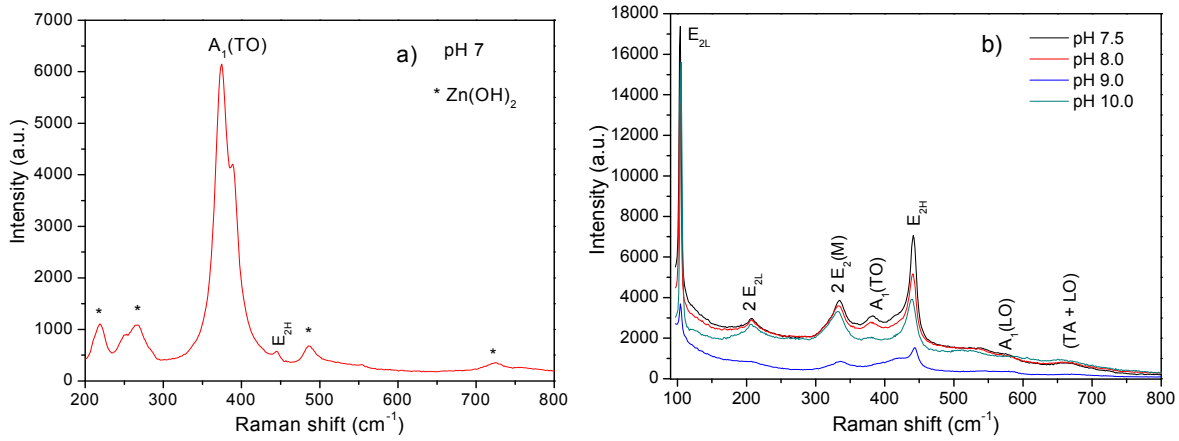

Fig. 5 Raman spectra of the ZnO nanostructures grown at (a) pH 7, and (b) other pH values of the reaction mixture

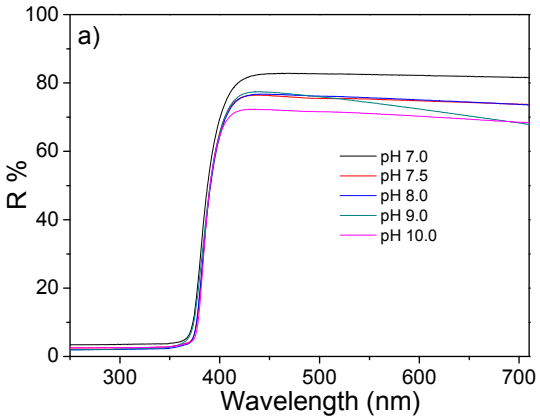

Fig. 6 (a) DRS spectra and their (b) Kubelka–Munk transformations used for the estimation of E_g of ZnO nanostructures grown at different pH values

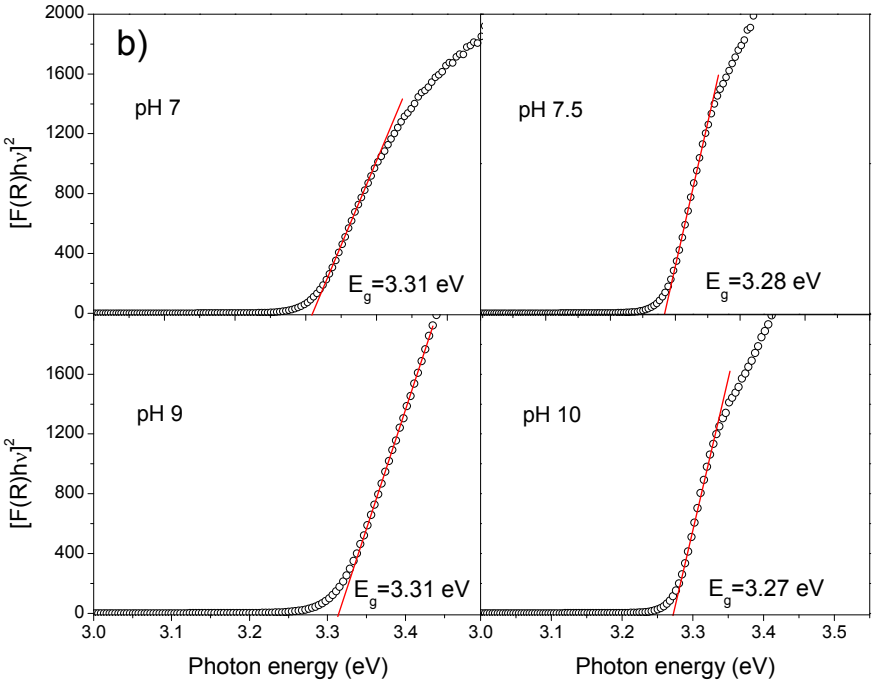

Fig. 6 Continued

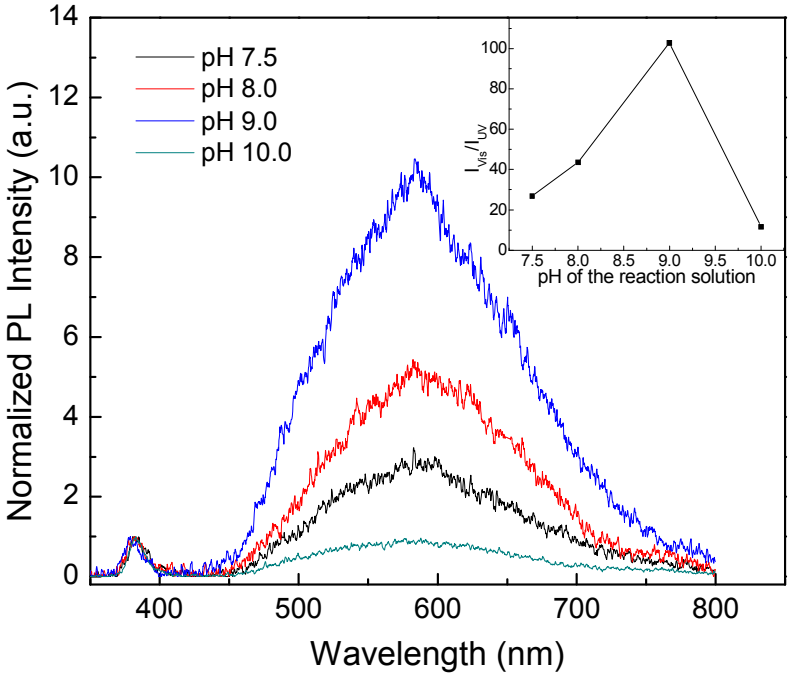

Fig. 7 Room temperature PL spectra of ZnO nanostructures grown at different pH values of reaction solution. The inset shows the variation of I_{Vis}/I_{UV} intensity ratio with solution pH

From the normalized PL spectra presented in Fig. 7, we can see that the relative intensity of the visible emission increases with pH value up to pH 9 and then suddenly decreases for pH 10 of the reaction mixture. The variation of intensity ratio (I_{Vis}/I_{UV}) with pH value presented as the inset of Fig. 7 clearly indicates that on increasing the pH of the reaction solution a higher amount of structural defects are incorporated into the ZnO nanostructures, in agreement with their XRD results presented earlier. Generally the nanostructures with higher specific surface area contain higher density of surface defects. On illuminating those nanostructures, photgenerated holes in the valence band are possibly trapped into the surface defects and are increasingly returned to the oxygen vacancies, causing an increase in the intensity of visible emission. Therefore, the increase in the intensity of the visible emission is probably due to higher surface area of the sample grown at pH 7.5, 8 and 9 (Table 1). The decreases in visible emission intensity for the sample grown at pH 10 is also in accordance with the reduction of its surface area as estimated from its adsorption-desorption isotherm. In fact, Samaele *et al*. (2010) have studied the effect of reaction solution pH on the morphology and optical properties of ZnO particles, observing a similar increase of visible PL emission with the increase of pH value, which they attributed to an increase of surface area due to morphology change (Samaele *et al.* 2010). On the other hand, Sharma *et al.* (2009) have studied the relationship between oxygen defects as oxygen vacancy (V_O^+) and O_2^- superoxide ions in their ZnO nanoparticles through PL spectroscopy, observing a similar trend as that of Samaele *et al.* (2010).

4. Conclusions

ZnO nanostructures of different morphologies could be fabricated by ultrasonic hydrolysis of zinc acetate in aqueous solution by controlling its hydrolysis rate through pH adjustment. While a solution pH 7 or lower produces impure ZnO nanostructures mixed with $Zn(OH)_2$ phase, higher pH values of the reaction mixture produce ZnO nanostructures in pure hexagonal phase. Controlling solution pH in between 7.5 and 10, phase pure ZnO nanostructures of varied morphology could be produced and the concentration of their structural and surface defects could be controlled. Utilization of low power ultrasound for the chemical synthesis of ZnO nanostructures efficiently has been demonstrated.

Acknowledgements

The work was partially supported by VIEP-BUAP (Grant # VIEP/EXC/2013) and CONACyT, Mexico (Grant # CB-2011/151767).

References

Alivisatos, A.P. (1996), "Semiconductor clusters, nanocrystals, and quantum dots", *Science,* **271**(5251), 933-937.

Arguello, C.A., Rousseau, D.L. and Porto, S.P.S. (1969), "First-order raman effect in Wurtzite-type crystals", *Phys. Rev.,* **181**(3), 1351-1363.

Bhattacharyya, S. and Gedanken, A. (2008), "A template-free, sonochemical route to porous ZnO nano-

disks", *Microporous and Mesoporous Materials*, **110**, 553-559.
Chiou, W.T., Wu, W.Y. and Ting, J.M. (2003), "Growth of single crystal ZnO nanowires using sputter deposition", *Diam. Relat. Mater.,* **12**, 1841-1844.
Cullity, B.D. (1956), "Elements of X-ray diffraction", *Addison-Wesley Publishing Company, Inc.*, **56**(10137), 98-99.
Demianets, L.N., Kostomarov, D.V., Kuz'mina, I.P. and Pushko, S.V. (2002), "Mechanism of growth of ZnO single crystals from hydrothermal alkali solutions", *Crystallogr. Rep.,* **47**(1), S86-S98.
Dhas, N.A. and Suslick, K.S. (2005), "Sonochemical preparation of hollow nanospheres and hollow nanocrystals", *J. Am. Chem. Soc.,* **127**, 2368-2369.
Escobedo-Morales, A. and Pal, U. (2008), "Defect annihilation and morphological improvement of hydrothermally grown ZnO nanorods by Ga doping", *Appl. Phys. Lett.,* **93**(19), 193120-1-193120-3.
Escobedo Morales, A., Sanchez Mora, E. and Pal, U. (2007), "Use of diffuse reflectance spectroscopy for optical characterization of un-supported nanostructures", *Revista mexicana de física*, **53**(5), 18-22.
Fan, Z. and Lu, J.G. (2005), "Gate-refreshable nanowire chemical sensors", *Appl. Phys. Lett.,* **86**, 123510-1-123510-3.
Hsu, J.W.P., Tallant, D.R., Simpson, R.L., Missert, N.A. and Copeland, R.G. (2006), "Luminescent properties of solution-grown ZnO nanorods", *Appl. Phys. Lett.,* **88**, 252103-1-252103-3.
Huang, M.H., Mao, S., Feick, H., Yan, H. Wu, Y., Kind, H., Weber, E., Russo, R. and Yang P. (2001), "Room-temperature ultraviolet nanowire nanolasers", *Science,* **292**, 1897-1899.
Jang, M.S., Ryu, M.K., Yoon, M.H., Lee, S.H., Kim, H.K., Onodera, A. and Kojima, S. (2009), "A study on the Raman spectra of Al-doped and Ga-doped ZnO ceramics", *Curr. Appl. Phys*., **9**, 651-657.
Janotti, A. and Van de Walle, C.G. (2007), "Native point defects in ZnO", *Phys. Rev. B.*, **76**, 165202-1-165202-22.
Jing, Z. and Zhan, J. (2008), "Fabrication and gas-sensing properties of porous ZnO nanoplates", *Adv. Mater.*, **20**, 4547-4551.
Kumar, R.V., Diamant, Y. and Gedanken, A. (2000), "Sonochemical Synthesis and Characterization of Nanometer-Size Transition Metal Oxides from Metal Acetates", *Chem. Mater.,* **12**(8), 2301-2305.
Kumar Yadav, H., Sreenivas, K., Katiyar, R.S. and Gupta, V. (2007), "Defect induced activation of Raman silent modes in rf co-sputtered Mn doped ZnO thin films", *J. Phys. D: Appl. Phys*., **40**, 6005-6009.
Laudise, R.A. and Ballman, A.A. (1960), "Hydrothermal synthesis of zinc oxide and zinc sulfide", *J. Phys. Chem.,* **64**, 688-691.
Lee, S.Y., Shim, E.S., Kang, H.S., Pang, S.S. and Kang, J.S. (2005), "Fabrication of ZnO thin film diode using laser annealing", *Thin Solid Films,* **473**, 31-34.
Mishra, P., Yadav, R.S., and Pandey, A.C. (2009), "Starch assisted sonochemical synthesis of flower-like ZnO nanostructure", *Digest Journal of Nanomaterials and Biostructures*, **4**(1), 193-198.
Morales-Flores, N., Pal, U. and Sanchez Mora, E. (2011), "Photocatalytic behavior of ZnO and Pt-incorporated ZnO nanoparticles in phenol degradation", *Applied Catalysis A: General*, **394**(1-2), 269-275.
Pal, U., Aguila Almanza, E., Vazquez, O., Koshizaki, N., Sasaki, T. and Terauchi, S. (2001), "Synthesis and characterization of Au/ZnO nanocompostes", *Modern Phys. Lett., B.,* **15**, 679-682.
Pal, U. and Santiago, P. (2005), "Controlling the morphology of ZnO nanostructures in a low-temperature hydrothermal process", *J. Phys. Chem. B.,* **109**, 15317-15321.
Pal, U., Kim, C.W., Jadhav, N.A. and Kang, Y.S. (2009), "Ultrasound-assisted synthesis of mesoporous ZnO nanostructures of different porosities", *J. Phys. Chem. C.*, **113**(33), 14676-14680.
Phan, T.L., Vincent, R., Cherns, D., Dan, N.H. and Yu, S.C. (2008), "Enhancement of multiple-phonon resonant raman scattering in Co-doped ZnO nanorods", *Appl. Phys. Lett.*, **93**(8), 082110-082113.
Pu, X., Zhang, D., Jia, L. and Su, C. (2007), "Synthesis of zinc oxide nanostructures with controlled morphologies using a simple sonochemical method", *J. Am. Ceram. Soc.*, **90**(12), 4076-4078.
Samaele, N., Amornpitoksuk, P. and Suwanboon, S. (2010), "Effect of pH on the morphology and optical properties of modified ZnO particles by SDS via a precipitation method", *Powder Technology*, **203**, 243-247.
Serrano, J., Romero, A.H., Manjon, F.J., Lauck, R., Cardona, M. and Rubio, A. (2004), "Pressure

dependence of the lattice dynamics of ZnO: An ab initio approach", *Phys. Rev. B.*, **69**(9), 094306-094319.
Sharma, P.K., Pandey, A.C., Zolnierkiewicz, G., Guskos, N. and Rudowicz, C. (2009), "Relationship between oxygen defects and the photoluminescence property of ZnO nanoparticles: a spectroscopic view", *J. Appl. Phys*., **106**(9), 094314-1-094314-5.
Studenikin, S.A., Golego, N. and Cocivera, M. (1998), "Fabrication of green and orange photoluminescent, undoped ZnO films using spray pyrolysis", *J. Appl. Phys.,* **84**(4), 2287-2294.
Suslick, K.S., Fang, M. and Hyeon, T. (1996), "Sonochemical synthesis of iron colloids", *J. Am. Chem. Soc.,* **118**(47), 11960-11961.
Vargas-Hernández, C., Jiménez-García, F.N. and Jurado, J.F. (2009), "Películas de ZnO impurificadas con Mn usando la Técnica silar", *Revista Latinoamericana de Metalurgia y Materiales,* **S1**(2), 501-506.
Venkatachalam, S., Kanno, Y. and Velumani, S. (2010), "Characterization on pulsed laser deposited nanocrystalline ZnO thin films", *Vacuum*, **84**, 1199-1203.
Venkateswara, K.R. and Sunandana, C.S. (2008), "Structure and microstructure of combustion synthesized MgO nanoparticles and nanocrystalline MgO thin films synthesized by solution growth route", *J. Mater Sci.,* **43**, 146-154.
Wahab, R., Kim, Y.S. and Shin, H.S. (2009), "Synthesis, characterization and effect of pH variation on zinc oxide nanostructures", *Mater. Transactions*, **50**(8), 2092-2097.
Wang, X., Xu, J., Yu, X., Xue, K., Yu, J. and Zhao, X. (2007), "Structural evidence of secondary phase segregation from the Raman vibrational modes in Zn1−xCoxO (0<x<0.6)", *Appl. Phys. Lett*., **91**(3), 031908-031910.
Wei, X.Q., Man, B.Y., Liu, M., Xue, C.S., Zhuang, H.Z. and Yang, C. (2007), "Blue luminescent centers and microstructural evaluation by XPS and Raman in ZnO thin films annealed in vacuum, N_2 and O_2", *Physica B.,* **388**, 145-152.
Wu, X.L., Siu, G.G., Fu, C.L. and Ong, H.C. (2001), "Photoluminescence and cathodoluminescence studies of stoichiometric and oxygen-deficient ZnO films", *Appl. Phys. Lett*., **78**(16), 2285-2287.
Xia, Y., Yang, P., Sun, Y., Wu, Y., Mayers, B., Gates, B., Yin, Y., Kim, F. and Yan, H. (2003), "One-dimensional nanostructures: Synthesis, characterization, and applications", *J. Ad*v. *Mater.,* **15**, 353-389.
Xu, C.X., Sun, X.W., Dong, Z.L. and Yu, M.B. (2004**), "**Zinc oxide nanodisk**",** *Appl. Phys. Lett.,* **85**(17), 3878-3880.
Xu, S. and Wang, Z.L. (2011), "One-dimensional ZnO nanostructures: solution growth and functional properties", *Nano Res*., **4**(11), 1013-1098.
Yao, B.D., Chan, Y.F. and Wang, N. (2002), "Formation of ZnO nanostructures by a simple way of thermal evaporation", *Appl. Phys. Lett.,* **81**(4), 757-759.
Zhang, J., Sun, L., Yin, J., Su, H., Liao, C. and Yan, C. (2002**), "**Control of ZnO morphology via a simple solution route**",** *Chem. Mater.,* **14**(10), 4172-4177.
Zhang, X., Zhao, H., Tao, X., Zhao, Y. and Zhang, Z. (2005), "Sonochemical method for the preparation of ZnO nanorods and trigonal-shaped ultrafine particles", *Mater. Lett.*, **59**, 1745-1747.
Zhou, H., Alves, H., Hofmann, D.M., Kriegseis, W., Meyer, B.K., Kaczmarczyk, G. and Hoffmann, A. (2002), "Behind the weak excitonic emission of ZnO quantum dots: ZnO/$Zn(OH)_2$ core-shell structure", *Appl. Phys. Lett.,* **80**(2), 210-212.
Zhu, Y.W., Zhang, H.Z., Sun, X.C., Feng, S.Q., Xu, J., Zhao, Q., Xiang, B., Wang, R.M. and Yu, D.P. (2003), "Efficient field emission from ZnO nanoneedle arrays", *Appl. Phys. Lett.,* **83**(1), 144-146.

CC